PCCP

Accepted Manuscript

ROYAL SOCIETY OF CHEMISTRY

www.rsc.org/pccp

Cite this: DOI: 10.1039/c0xx00000x

www.rsc.org/xxxxxx

ARTICLE TYPE

The Synergistic Mechanism of Graphene and MoS_2 for Hydrogen Generation: Insights from Density Functional Theory

Yanli Yuan, Xiping Gong and Hongming Wang*

Received (in XXX, XXX) Xth XXXXXXXXX 20XX, Accepted Xth XXXXXXXXX 20XX

DOI: 10.1039/b000000x

The synergistic effect of the graphene and MoS_2 was investigated by using density functional theory (DFT) calculations on the enhanced photocatalytic H_2 production activity of TiO_2/graphene/MoS_2 ternary nanoparticle. Our results indicate that it can form a weak covalent bond between the Ti atom of TiO_2 nanocluster and the nearest C atom on graphene, which not only makes the original degenerate C(2p) orbital level of the graphene (part of the conduction band energy level) split, resulting in the production of a lower level of C(2p) that is easier to accept the excited electron from the Ti(3d) orbital, but also forms a +/- sequence electric field in the interface between them. It is conducive that the electron moves from the TiO_2 cluster to the graphene. In addition, we also find that the band gap of the TiO_2 cluster can be doped by the graphene and MoS_2, and the conduction band consists predominantly of C(2p), S(3p) and Mo(4d) orbital energy level near the Fermi level. These results illustrate the excited electron will eventually accumulate in the graphene or MoS_2 film, which can effectively enhance the separate between the excited electrons and the holes in TiO_2 clusters, thereby to increase the efficiency of hydrogen evolution. Our results are consistent with the experimental results, and can provide some valuable information for the design of photocatalytic composites.

1. Introduction

Converting solar energy into hydrogen is considered to be a valid strategy to solve the energy crisis.[1-4] It is effective to use the heterogeneous photocatalytic materials for hydrogen generation, because it can strengthen the separation of photo-excited electrons and holes in the semiconductor (such as Titanium dioxide (TiO_2)), and then the hydrogen evolution and oxygen evolution reaction can be occurred at the electrons and holes on the corresponding surface of the photocatalysts, respectively.[5-7] So, some comprehensive reviews have summarized the heterogeneous photocatalytic materials during the latest decade. [8-10]

In recent years, graphene-based heterogeneous photocatalytic materials are attracted considerable attentions. This is mainly due to a unique sp^2 hybrid carbon network resulting in many of highly significant features, such as the ultrafast electron mobility at room temperature (200000 $cm^2V^{-1}s^{-1}$), the conductivity (10^6 Scm^{-1}), the large surface area of the theoretical (~2600 m^2g^{-1}) and the high work function (4.42 eV), etc.[11-13] These excellent properties of graphene showed great potential to become the component of the photocatalysts for hydrogen generation. Therefore, many researchers focus on ternary and/or multicomponent photocatalysts containing photocatalysts, graphene and cocatalyst. For example, Hou *et al* developed the CdS QDs/graphene/$ZnIn_2S_4$ system exhibited highly efficient hydrogen production because of the high hydrothermal stability and efficient electron transfer, and that emphasized the importance of semiconductor heterostructure as an effective photocatalysts. [14] It is worth mentioning that the interfacial electron transfer capability can be enhanced significantly and the band structure of the photocatalysts can be doped by the graphene, facilitating the charge separation efficiently at different energy levels. Meanwhile, the cocatalyst containing abundant elements like the Ni, Co and Fe can serve as electron collector and active sites for the hydrogen evolution reaction. [9,15,16] Graphene can also play a role of the cocatalyst, and constitute a synergistic effect, with the other cocatalysts, on improving the photocatalytic efficiency.[17-19] Recently, Yu *et al* [17a] firstly proposed a three-component composite TiO_2/graphene/MoS_2 containing 0.25wt% graphene. The results show that graphene acts as an electron reservoirs, and MoS_2 can act as a source of active adsorption sites, to achieve synergetic highly efficient H_2 evolution with the H_2 production rate of 165.3 $\mu mol \cdot h^{-1}$ which is 75 times that of the TiO_2/MoS_2 [17b]. Very recently, Lin *et al* [19] demenstrated that ZnS loaded with 0.25 wt% graphene and 2 atom**%** MoS_2 reached a high H_2-evolution rate of 2258 $\mu mol \cdot h^{-1}$ which is about 2 times that of ZnS alone. Several review articles have also summarized the latest developments related to graphene-based photocatalysts, and consider that the main reasons why that significantly enhance the photocatalytic efficiency have three main aspects: (1) it can form the space potential difference promoting the photogenerated electron-hole separation effectively; (2) it can tune the bandgap by changing the band structure of the photocatalysts; (3) it can provide catalytic reaction sites for the hydrogen evolution reaction. [20,21]

From the existing researches, the introduction of graphene is able to lead to a significant improvement on the photocatalytic H_2 production activity. However, the roles of graphene, synergistic effects of various components and the interfacial charge transfer process in ternary photocatalysts remain unclear. And the mechanism of enhancing the photocatalytic efficiency is still unsharp at this stage. So, it is necessary to carry out the detailed investigations on electronic properties electron transfer of ternary photocatalysts. This would give valuable information for the design and synthesis of ternary photocatalysts in the future.

In this work, we investigate the electronic structure properties of the ternary photocatalysts (a case study of TiO_2/graphene/MoS_2), and characterize the synergistic effects of different components and the interfacial charge transfer process of photocatalysts by using the density functional theory (DFT) calculations. We found that it can form a weak covalent bond between the TiO_2 cluster and graphene, and the interface between graphene and TiO_2 cluster can form a +/- sequence electric field. The band gap of the TiO_2 cluster can be doped by the graphene and MoS_2. These results illustrate that the electron moves from the TiO_2 cluster to graphene, and eventually accumulate in the graphene or MoS_2 film.

2. Computational methods

All the calculations including geometry optimization and electronic structure calculations are performed by using first-principles DFT,[22-25] implemented with the Spanish Initiative for Electronic Simulation with Thousands of Atoms (SIESTA) code.[26,27] A localized basis set composed of double zeta plus polarization (DZP) was used. The standard norm-conserving Troullier-Martins pseudopotential in the fully nonlocal (Kleinman-Bylander) form was employed. We described the exchange and correlation effects using the generalized gradient approximation (GGA) exchange-correlation function[28] developed by Perdew, Burke and Ernzerh.[29] The real space mesh cutoff was set to more than 200Ry, The Monkhorst-Pack[30] special k-point was set to 5×5×1, and the k-point was set to 9×9×1 on the density of state(DOS) calculation to achieve higher accuracy. We use the conjugated gradient (CG) minimization technique to obtain the optimized structure until the maximum atomic force is smaller than 0.04 eV / Å and the atomic positions were fully relaxed without constraint.

In our simulation, the interface between graphene and MoS_2 is modeled by using a supercell in the x-y plane(Figure. 1). We build the 14.76 × 14.76 Å lateral periodicity of the graphene including 72 atoms and 15.83 ×15.83 Å lateral periodicity of the MoS_2 monolayer including 75 atoms, and the lattice mismatch is 6.8%. After configuration optimization, the last lattice parameters of MoS2/grapheme system is 15.33 × 15.32 Å in the x-y plane. The vacuum space at z axes is 20 Å in the direction normal to the interface, representing the isolated slab boundary condition. The lattice of $MoS_2$was set to match to that of graphene in the supercell. The supercells are then fully relaxed for both the lattice constants and the atomic geometry. The $(TiO_2)_3$ configuration contains all the classical features of the well-understood R(101) surface of anatase TiO_2 which has been widely used in the literature[31], and the results are in good agreement with the experimental data. In order to understand the photocatalytic hydrogen production synergistic mechanisms by comparing TiO_2/graphene/MoS_2 system, we also calculated the two other systems (TiO_2/graphene and graphene/MoS_2); whose lattice parameters and calculated parameters is the same as the TiO_2/graphene/MoS_2 system. To find the most favorable adsorption configurations, the $(TiO_2)_3$ cluster was made initially to approach the graphene sheet in different positions, and various possible adsorbing orientations were investigated. After full relaxation, the optimized configurations obtained from the different initial states were compared, and the most stable configurations is shown in Fig. 1 with the Ti2 atom located above the C-C bond of graphene.

To reflect the combination of these three systems stability, we calculated the binding energy（E_b）of the TiO_2/graphene/MoS_2 system, which are showed as fellow:

$$E_{b1} = E_{tot}[TiO_2/graphene/MoS_2] - E_{tot}[graphene/MoS_2] - E_{tot}[TiO_2] \quad (1)$$

$$E_{b2} = E_{tot}[TiO_2/graphene/MoS_2] - E_{tot}[TiO_2/geaphene] - E_{tot}[MoS_2] \quad (2)$$

$$E_{b3} = E_{tot}[TiO_2/graphene/MoS_2] - E_{tot}[MoS_2] - E_{tot}[graphene] - E_{tot}[TiO_2] \quad (3)$$

Here, $E_{tot}[TiO_2/graphene/MoS_2]$, $E_{tot}[graphene/MoS_2]$ and $E_{tot}[TiO_2/geaphene]$ are the total energies per supercell of the TiO_2/graphene/MoS_2, graphene/MoS_2 and TiO_2/graphene systems, respectively. $E_{tot}[TiO_2]$, $E_{tot}[MoS_2]$ and $E_{tot}[graphene]$ are those for isolated TiO_2 cluster, isolated MoS_2 and isolated graphene respectively. The isolated TiO_2 cluster reference energy has been computed in a 30Å×30Å×30Å cell.

To analyse the nature of the TiO_2/graphene/MoS_2 interaction, we also have examined electron density differences at the interface, $\Delta\rho(r)$ and the planar-averaged density difference, $\Delta\rho^{avg}(z)$ here defined as:

$$\Delta\rho(r) = \rho_{tot}[TiO_2/graphene/MoS_2] - \rho_{tot}[MoS_2] - \rho_{tot}[graphene] - \rho_{tot}[TiO_2] \quad (4)$$

$$\Delta\rho^{avg}(z) = \int_{\sum(z)} dxdy\Delta\rho = \sum_{ij} \Delta x_i \Delta y_j \Delta\rho_{i,j} \quad (5)$$

$\rho_{tot}[TiO_2/graphene/MoS_2]$ is the electron densities of TiO_2/graphene/MoS_2, $\rho_{tot}[MoS_2]$, $\rho_{tot}[graphene]$ and $\rho_{tot}[TiO_2]$ are those for the MoS_2, graphene and TiO_2 systems, respectively. The plan averaged electron density difference is obtained by integrating the electron density differences along x-y plane, where the z axis is along the surface normal direction and x/y is the cross-section of the supercell in the x-y plane at z, the i and j are one point divided lattice axis and b-axis lattice, respectively.

3. Results and discussions

3.1. Geometric structures and binding energies

To explore the roles of graphene and MoS_2 nanocluster in this ternary photocatalysts, it is necessary to consider the three systems: (a) TiO_2/graphene, (b) graphene/MoS_2 and (c) TiO_2/graphene/MoS_2. The optimized configurations are shown in Figure 1. In three arrangements, graphene keeps its plane and hexagonal atomic network，which is consistent with the previous research[32]. From the binding energies and the interfacial distances of the three optimized structures, Table 1, it can be found that there is no strong interaction between the TiO_2 cluster (or MoS_2)

and graphene which consists with the previous theoretical result. The binding energy of TiO_2/graphene (-3.43 eV) is greater than that of MoS_2/graphene (-1.19 eV). So it is easier for graphene to combine TiO_2 cluster than MoS_2. The binding energy of TiO_2/graphene/MoS_2 is less than that of TiO_2/graphene, indicating that MoS_2 can affect the combination between TiO_2 and graphene. This conclusion is in agreement with the distance between TiO_2 and graphene below. To obtain accurate van der Waals energies, the van der Waals density functional (vdW-DF) as proposed by Dion et al.[32] and recently implemented in the SIESTA code[33] was used to check the binding energy. The derivation of binding energy with vdW-DF is within 0.05eV compared with the GGA method (Table 1). It is noted that the implement of calculation van der Waals Force is ineffective at present state.

Table1: the binding energy (E_b), the interfacial distance D in the three optimized structure.

	E_b(eV)	$E_{b\ vdW}$(eV)	D (Å)
TiO_2/graphene	-3.43[a]	-3.38[a]	2.43 [c]
graphene/MoS_2	-1.19[b]	-1.16[b]	3.80[d]
TiO_2/graphene/ MoS_2.	-2.66[a]	-2.62[a]	2.40[c] / 3.84[d]

[a] Binding energy between TiO_2 and graphene, [b] binding energy between MoS_2 and graphene, [c] the shortest distance between the TiO_2 cluster and the graphene, [d] the shortest distance between the MoS_2 nanocluster and the graphene.

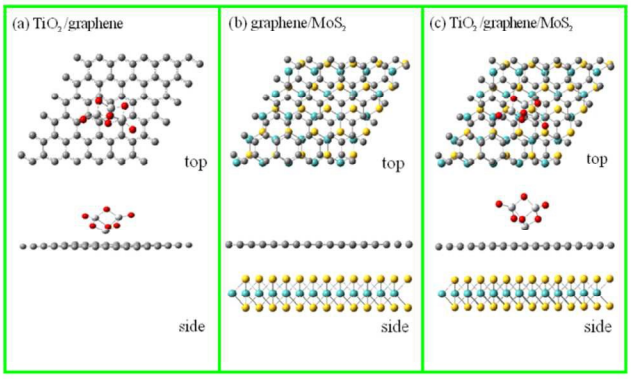

Figure 1. The top and side view of the optimized structure of the three composites: (a) TiO_2/graphene, (b) graphene/MoS_2 and (c) TiO_2/graphene/MoS_2. The red, white, grey, yellow and blue represent O, Ti, C, S, Mo, respectively.

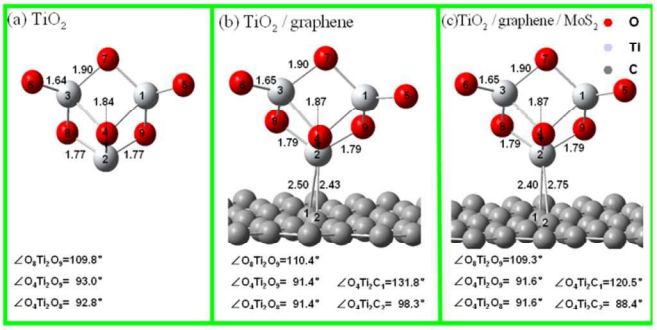

Figure 2. The bond distances and angles between $(TiO_2)_3$ and graphene in the optimized structures of (a) $(TiO_2)_3$cluster, (b) graphene/ TiO_2 and (c) TiO_2/graphene/MoS_2.

To quantitatively characterize the interaction between TiO_2 nanocluster and graphene, we draw the bond lengths and angles between $(TiO_2)_3$ and graphene among the optimized structures, which are shown in Figure 2. As seen from Figure 2a, TiO_2 nanocluster has C_2 symmetry. The shortest and longest bond lengths of Ti-O are 1.64 Å(Ti3-O6) and 1.90 Å(Ti3-O7) in TiO_2 nanocluster, respectively. The Ti2 atom is located at the bridge site between TiO_2 nanocluster and graphene in the TiO_2/graphene and TiO_2/graphene/MoS_2 composites. In the TiO_2/graphene system, Figure 2b, TiO_2 keeps the same symmetry as that in Figure 2a. However, compared with the TiO_2 nanocluster, the bonds near the graphene increase a little and the bonds far from graphene have no change. This indicates that graphene affects TiO_2 nanocluster mainly by the interaction with the adjacent Ti2 atom. In the TiO_2/graphene/MoS_2 system, Figure 2c, the structure of the TiO_2 nanocluster is consistent with that in TiO_2/graphene system, which shows that the introduction of MoS_2 almost has no effect on the structure of TiO_2 nanocluster. From the distances between Ti2 atom and C_1/C_2 atoms of graphene in both Figure 2b and 2c, it can be inferred that there is weak interaction between TiO_2 and graphene.

Meanwhile, we also investigated some key bond angles formed by Ti2 atom with the surrounding O atoms and C atoms in three systems, respectively. As shown in Figure 2, there are little changes of angles $\angle O_8Ti_2O_9$, $\angle O_4Ti_2O_9$ and $\angle O_4Ti_2O_8$ in the three optimized structures. But the angles $\angle O_4Ti_2C_1$ and $\angle O_4Ti_2C_2$ are 131.8° and 98.3° in TiO_2/graphene system, which differs from those (120.5° and 88.4°) in TiO_2/graphene/MoS_2 system. From Figure 2, the O8, O9, Ti2 and C2 atoms form an approximate plane, and the Ti2-O_4 bond is substantially perpendicular to the plane. This means that the 3d orbital of Ti2 atom is hybridized. It is probable that there is an overlap between the Ti2-3d orbital and the C2-$2p_z$ ortital which is perpendicular to the graphene plane. This helps to explain the weak interaction between graphene and TiO_2 cluster.

3.2 Charge density difference

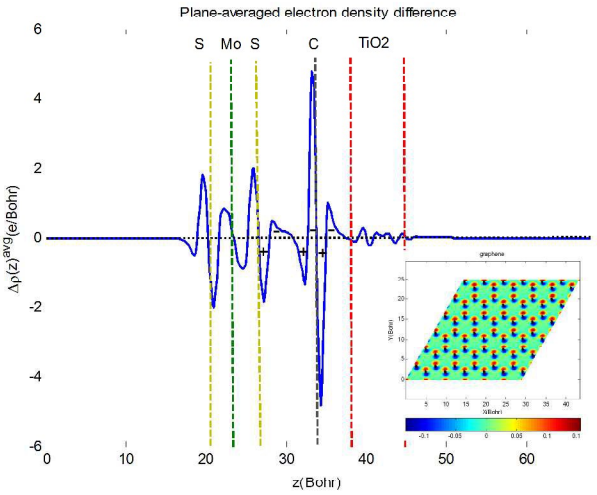

Figure.3. Plane-averaged electron density difference of the TiO_2/graphene/MoS_2 system along the vertical axis (z axis).The coloured

dash lines indicate the positions of each composite, and the $\Delta\rho^{avg}(z)>0$ represents the charge accumulation. The insert is the electron density differences at the graphene surface, and these dark dots represent the C atoms on graphene

In order to give more detailed understandings of the interface in TiO_2/graphene/MoS_2 system, we plot the plane-averaged electron densities and electron density differences (Figure 3). From Figure 3, it can be seen clearly that graphene is polarized due to TiO_2 and MoS_2 cluster. To further verify this phenomenon, we draw the charge density difference of the surface of graphene. It is obvious that each C atom on graphene is polarized, which forms +/- sequence electric field with the intensity of about 0.1 e/Bohr^{3}S. From the charge polarization of graphene, it is found that charge accumulation occurs on the graphene surface close to MoS_2 and charge depletion happens on the other side close to TiO_2. In the interface between the graphene and the TiO_2 nanocluster, the Ti2 atom is electron withdrawing, resulting in the electron depletion in C atom of the graphene and the electron accumulation in Ti2 atom which forms a +/- sequence electric field finally. It is conducive that the electron moves from the TiO_2 nanocluster to graphene. For the interface between MoS_2 and graphene, the S atom of MoS_2 nearby the graphene are also polarized to form a +/-/+/- sequence electric field. Although the interaction between MoS_2 and graphene is very weak, a significant electron accumulation is observed in the interlayer region. It indicates that charge transfer is induced between the graphene and the MoS_2 surface, which is also consistent with that of the reference[34]. Although the large distance between graphene and MoS_2 is able to have slightly effects on the electron transfer from graphene to the MoS_2 surface, it can attract more electrons due to the much more depletion of the MoS_2 surface. So, as a result, it does not preclude the charge transfer between graphene and the MoS_2 surface.

3. 3. The projected density of states (PDOS) of the composites

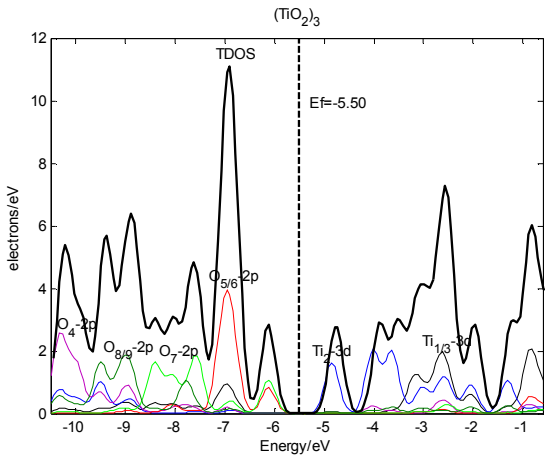

Figure 4. Projected density of states (PDOS) onto the $(TiO_2)_3$ cluster. The dashed line indicates the Fermi energy level (Ef).

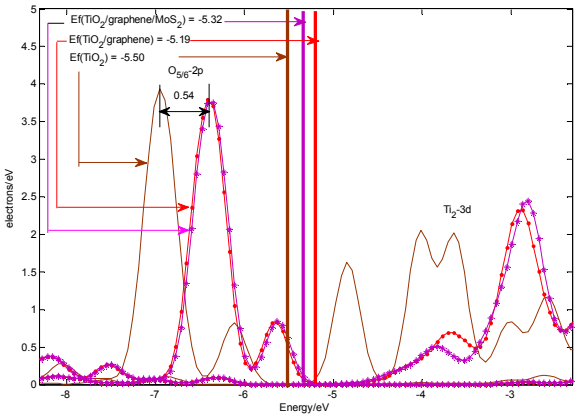

Figure 5. Projected density of states (PDOS) of the $O_{5/6}$-2p and Ti_2-3d of the $(TiO_2)_3$ cluster in the three composites: (a) TiO_2, (b) TiO_2/graphene and (c) TiO_2/graphene/MoS_2. The coloured middle lines represent the Fermi level, and the same colour line represents the same system. The left nearby the Fermi level is $O_{5/6}$-2p PDOS, and the right is Ti_2-3d PDOS for each composites.

To inquire into the electronic coupling and orbital contributions in the calculated systems, the projected density of state (PDOS) for three calculated systems would be probed. It shows the total density of states (TDOS) of $(TiO_2)_3$ nanocluster and each valence electron orbit of Ti and O atoms in Figure 4. As from Figure 4, the valence band of the TiO_2 nanocluster is composed mainly of the O5/6 2p orbitals (O5/6 represented the 5th and 6th O atoms), and the conduction band is mainly composed of Ti2-3d orbital. The band gap calculated by using GGA and LDA+U is only 1.36 and 1.68 eV, respectively, and is far less than the experimental value (~3.2eV). [35] It is caused by three main reasons: (1) the well-known shortage that DFT underestimates the band gap due to the self-correlation error of electrons and inherent lack of derivative discontinuity; (2) the difference existed between a small cluster and bulk matter because of the size effect[31,35,36]. Besides, as shown in Figure 4, the electron numbers are not the same for some O-2p and Ti-3d orbitals. This is because there are two types of Ti atoms and four types of O atoms of different environments, Figure 2. The closer to the Fermi level, the more of the electrons is. Furthermore, combined with the TiO_2 cluster structure in Figure 2a, on the one hand, we found that the O5/6 atoms not meet the eight electron configuration, so that they have high reactivity with unpaired electrons. So it is easy for O5/6-2p energy levels to close to the Fermi level. On the other hand, the Ti2-3d energy level is closest to the conduction band among all the Ti-d energy levels. It can be seen that the Ti2 atom also does not reach a stable outer electron configuration from Figure 2. Because of the atoms unreached stable configuration on the surface of the $(TiO_2)_3$ cluster, the number of electrons nearby the Fermi level increase. It can reduce the energy required for the being excited electrons.

In order to understand the impact of graphene and MoS_2 on the O-2pTi-3d orbitals and the Fermi level in $(TiO_2)_3$ nanocluster, we also plot the O5/6-2p and Ti2-3d PDOS for the three calculated systems in Figure 5. Compared to the isolated TiO_2 nanocluster system, it can be seen the graphene has more significant effects on O-2p and Ti-3d of the TiO_2 cluster than the MoS_2 in the TiO_2/graphene and TiO_2/graphene/MoS_2 system. On one hand,

because of introduction of graphene, the O-2p orbital peak level shifts to the right by 0.54 eV. The corresponding Fermi level shifts by 0.31eV. So the graphene make the O5/6 peak energy level closer to the Fermi level. Besides, the influence of graphene on Ti2-3d peak energy level is more obvious. It can be seen clearly that the Ti2-3d peak energy level in the TiO_2/graphene system shifts to the right, and the peak changes dramatically. The main reason is that the Ti2-3d orbital interacts with the C1/C2-2p orbital of the graphene, making the Ti2-3d orbital energy level more localized at the higher level. On the other hand, the MoS_2 almost does not take any effect on shifting the O5/6 energy level. Though MoS_2 shows larger influence the impact on Ti2-3d peak energy level than that on O5/6-2p peak energy level, this influence is small compared to that resulted by graphene. However, it is interesting that the MoS_2 makes the Fermi level moves to the left by 0.14 eV. This show the O5/6-2p orbitals of the TiO_2/graphene/MoS_2 is closer to the Fermi level compared with that in the TiO_2/graphene system, which means that the electrons on $O_{5/6}$-2p orbitals of TiO_2/graphene/MoS_2 are more likely to be excited by the light. Apart from the O5/6 and Ti2 atoms, it can show the consistency for the analysis of other O and Ti atoms. On the whole, the graphene and MoS_2 can both make O-2p orbit closer to the Fermi level, especially the graphene. This indicates that they have the synergistic influence on making electrons of the O-2p be more easily excited to the conduction band.

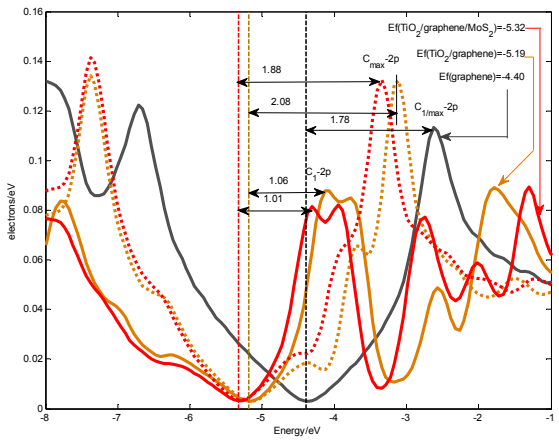

Figure 6. Projected density of states (PDOS) of the C_1-2p and C_{max} -2p of the graphene in the three composites: (a) graphene, (b) TiO_2/graphene and (c) TiO_2/graphene/MoS_2. Middle coloured dotted line represents the corresponding with the Fermi level position; the same colour line represents the same system.

To clearly understand the process of the excited electrons excited to the graphene by the covalent band formed Ti2 and the nearest C atoms (marked C_1 atom), we studied the influence of TiO_2 and MoS_2 on C-2p orbital of graphene. As can be seen from Figure 6, the TiO_2 and MoS_2 can affect C_1/C_{max}-2p (C_{max} is the C atom that has the maximum peak energy level). The peak energy levels of C-2p are the same in pure graphene system, but they show the difference in TiO_2/graphene or TiO_2/graphene/MoS_2 system with the value and shape of C_1-2p changed significantly. For the C_1 atoms in TiO_2/graphene, the main peak is spitted into two main peaks (peak energy values are -4.128and -1.784 eV, respectively), and the energy integral value of the conduction band near the Fermi level is larger than that of the other C atoms. The interaction between Ti2-3d and C1-2p orbitals leads to the C1-2p orbital localized and making the energy level closer to the Fermi level. For the C_1 atoms in TiO_2/graphene/MoS_2, the main peak is spitted into three peaks (peak energy values are -4.309, -2.745 and -1.303eV, respectively). It not only reflects the interaction between C1-2p and Ti2-3d orbital, but also shows the MoS_2 also have an influence on C1-2p orbital. Meanwhile the MoS_2 also makes C1-2p orbital slightly offset to the left. Besides, the Fermi level is shifted to the left for the TiO_2/graphene or TiO_2/graphene/MoS_2 systems. The difference is 1.78eV between the C-2p orbital peak energy level and the Fermi level for pure graphene; while the maximum/minimum difference for the TiO_2/graphene and TiO_2/graphene/MoS_2 systems are the 2.08/1.01eV and 1.88/1.01eV, respectively. This shows that the sp^2 orbital are destroyed by the TiO_2 clusters and MoS_2 splitting into lower and higher located C-2p orbital levels. Overall, the Ti1 atom makes the main distinct peak of the C-2p orbital spitting into more peaks, resulting in a lower localized C-2p orbital; while the MoS_2 can make C-2p level shift toward the Fermi level.

To further explore the component of the valence and conduction band of the TiO_2/graphene/MoS_2 and the process of charge transfer, we also draw the PDOS of the TiO_2/graphene/MoS_2 Figure 7.

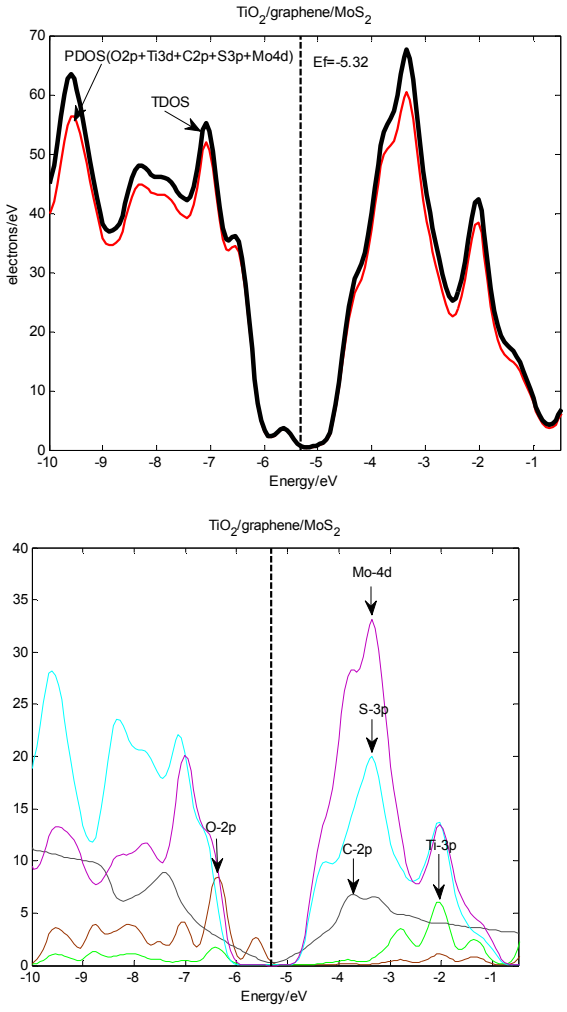

Figure 7. The Total density of states(TDOS)(left) and Projected density of states (PDOS)(right) of the TiO_2/graphene/MoS_2, middle dotted line represents the corresponding with the Fermi level position, each of the major peaks is pointed by the arrow.

From the up picture in Figure 7, the components of the valence and conduction band compose mainly of O-2p, Ti-3d, C-2p, S-2p and Mo-4d orbitals. The valence band is O-2porbital, and the conduction band are C-2p, S-3p and Mo-4d Composition. The band gap of $(TiO_2)_3$ nanocluster, TiO_2/graphene and TiO_2/graphene/MoS_2 system are 1.36, 0.80 and 0.02eV, respectively. This indicates that the band gap of semiconductor photocatalysts can be adjusted by doping other material, such as the graphene and MoS_2. From Figure 7, it can be seen that the C-2p, S-3p and Mo-4d peaks exist between the O-2p and Ti-3d energy levels. This provides a sign that the excited electrons eventually appear in the C-2p, S-3p and Mo-4d energy levels. That can effectively enhance the separate between the excited electrons and the holes in TiO_2 clusters, thereby to increase the efficiency of hydrogen evolution. Our calculation results agree with the experimental results.[17a]

4. Conclusions

In summary, DFT calculations were performed to investigate the heterogeneous TiO_2/graphene/MoS_2. The geometric structures and electrons properties were calculated to clarify the interface interaction in electronic level. And also, graphene and MoS_2 in the enhanced photocatalytic H_2 production activity of TiO_2 nanoparticle was hold key roles. Based on the analysis of the calculation results, we obtain the following conclusions.

(1) The graphene and MoS_2 can make O-2p orbital closer to the Fermi level, especially the graphene, indicating that they have the synergistic effect on making electrons of the O-2p more easily excited to the conduction band. (2) It can form a covalent bond between the Ti atoms of TiO_2 nanoclusters and the nearest C atoms on graphene, resulting in the production of a lower C-2p energy level, which is easier to accept the excited electron from the Ti-3d orbital. (3) The interface between the graphene and the Ti atoms of TiO_2 cluster can form a +/- sequence electric field. It is conducive that the electron moves from the TiO_2 cluster to the graphene. (4) The band gap of the TiO_2 cluster can be doping by the graphene and MoS_2. In addition, the conduction band consists predominantly of C-2p, S-3p and Mo-4d orbital energy level near the Fermi level, it illustrates the excited electron will eventually accumulate in the graphene or MoS_2 film.

Acknowledgements

The support of the National Natural Science Foundation of China (21363014 and 21103082) is gratefully acknowledged.

Notes and references

[a] *Institute for advanced study, Nanchang University, Nanchang , 330031,China. Fax: 0086-791-83969963; Tel: 0086-791-83969963; E-mail: Hongmingwang@ncu.edu.cn*

1. N. S.Lewis, D. G. Nocera, Proceedings of the National Academy of Sciences of the United States of America, 2006, 103, 15729-15735.
2. X. B. Chen, S. H. Shen, L. J. Guo, S. S. Mao, Chemical Reviews, 2010, 110, 6503-6570.
3. K. Maeda, K. Domen, Journal Of Physical Chemistry Letters, 2010, 1, 2655-2661,
4. H. J. Jeong, H. Y. Kim, H. Jeong, J. T. Han, S. Y. Jeong, K. J. Baeg, M. S. Jeong, G. W. Lee, Small 2014, 10. 2057-2066.
5. H. W. Bai, Z. Y. Liu, D. D. Sun, International Journal of Hydrogen Energy, 2012, 37, 13998-14008.
6. Z. Wei, Y. Li, S. Luo, C. Liu, D. Meng, M. Ding, G. Zeng, Separation and Purification Technology,2014, 122, 60-66.
7. U. Gupta, B. G. Rao, U. Maitra, B. E. Prasad, C. N. R. Rao. Chemisty-An Asian Journal, 2014, 9, 1311-1315.
8. Kudo, Y. Miseki,. Chemical Society Reviews, 2009, 38, 253-278.
9. R. Marschall, Advanced Functional Materials, 2014, 24, 2421-2440.
10. S. Liu, X. J.Zhao, C. Terashima, A. Fujishima, K. Nakata, Physical Chemistry Chemical Physics, 2014, 16, 8751-8760.
11. K. S. Novoselov, A. K. Geim, S.V. Morozov, D. Jiang, Y. Zhang, S. V. Dubonos , I.V. Grigorieva, A. A. Firsov, Science, 2004, 306, 666-669.
12. X. An, J. C. Yu, Rsc Advances, 2011, 1, 1426-1434.
13. H. Tang, C. M. Hessel, J. Wang, N. Yang, R. Yu, H. Zhao, D. Wang,. Chemical Society Reviews, 2014, 43, 4281-4299.
14. J. Hou, C. Yang, H. Cheng, Z. Wang, S. Jiao, H. Zhu. Physical Chemistry Chemical Physics, 2013, 15, 15660-15668.
15. J. Ran, J. Zhang, J.G. Yu, M. Jaroniec, S. Z. Qiao,. Chemical Society Review, 2014, doi:10.1039/c3cs60425j.
16. J. H. Yang, D. G.Wang, H. X. Han, C. Li. Accounts of Chemical Research, 2013, 46, 1900-1909.
17. (a) Q. J.Xiang, J. G. Yu, M. Jaroniec. Journal of the American Chemical Society, 2012, 134, 6575-6578. (b) S. Kanda, T. Akita, M. Fujishima, H. Tada, Journal of Colloid and Interface Science, 2011, 354, 607-610. S . Zhuang, X. Xu, B. Feng,J. Hu, Y. Pang, G. Zhou, L. Tong, Y. Zhou, Acs Applied Materials & Interfaces, 2014, 6, 613-621.
18. B. L.Zhu, B. Z. Lin, Y. Zhou, P. Sun, Q. R. Yao, Y. L. Chen, B. F. Gao, Jouranal of Materials Chemistry A, 2014, 2, 3819-3827.
19. Q. J. Xiang, J. G. Yu, Journal of Physical Chemistry Letters, 2013, 4, 753-759.
20. G. Xie , K. Zhang , B. Guo, Q. Liu, L. Fang, J.R. Gong, Advanced Materials, 2013, 25, 3820-3839.
21. P. Hohenberg, W. Kohn, Physical Review, 1964, 136, B864-B871.
22. W. Kohn, W. L. J. Sham, Physical Review, 1965, 140, A1133-A1138.
23. Perdew , A. Zunger , Physical Review B 1981, 23, 5048-5079.
24. D.-e. Jiang , B. G. Sumpter , S. Dai , The Journal of Physical Chemistry C, 2006, 110, 23628-23632.
25. P. Ordejon, E. Artacho, J. M. Soler, Physical Review B, 1996, 53, 10441-10444 .
26. M. Soler, E. Artacho, J. D. Gale, A. Garcia, J. Junquera, P. Ordejon, D. Sanchez-Portal. Journal of Physics-Condensed Matter, 2002, 14, 2745-2779.
27. J. P. Perdew, J. A. Chevary, S. H. Vosko, K. A. Jackson, M. R. Pederson, D. J. Singh, C. Fiolhais, Physical Review B, 1992, 46, 6671-6687.
28. J. P. Perdew, K. Burke, M. Ernzerhof, Physical Review Letters, 1996, 77, 3865-3868.
29. H. J. Monkhorst, J. D. Pack, Physical Review B, 1976, 13, 5188-5192.
30. W. Geng, H. X. Liu, X. J. Yao, Physical Chemistry Chemical Physics, 2013, 15, 6025-6033.
31. Y. D. Ma, Y. Dai, M. Guo, C. W. Niu, B. B. Huang, Nanoscale, 2011, 3, 3883-3887.
32. M. Dion, H. Rydberg, E. Schröder, D. C. Langreth and B. I. Lundqvist, Phys. Rev. Lett., 2004, 92, 246401.
33. G. Román-Pérez and J. M. Soler, Phys. Rev. Lett., 2009, 103, 096102
34. J. Bard, M. A. Fox, Accounts of Chemical Research, 1995, 28, 141-145.
35. P. Mori-Sanchez, A. J. Cohen, W. T. Yang, Physical Review Letters, 2008, 100, 146401.

36. L. J. Sham, M. Schluter, Physical Review Letters, 1983, 51, 1888-1891.